ACS Catalysis

Letter

pubs.acs.org/acscatalysis

Electrocatalysis on Oxide-Stabilized, High-Surface Area Carbon Electrodes

Manuel A. Méndez, Leila Alibabaei, Javier J. Concepcion, and Thomas J. Meyer*

Department of Chemistry, University of North Carolina at Chapel Hill, Chapel Hill, North Carolina 27599, United States

Supporting Information

ABSTRACT: A procedure is described for preparing and derivatizing novel, high surface area electrodes consisting of thin layers of nanostructured ITO (Sn(IV)-doped indium tin oxide, *nano*ITO) on reticulated vitreous carbon (RVC) to give RVC|*nano*ITO. The resulting hybrid electrodes are highly stabilized oxidatively. They were surface-derivatized by phosphonate binding of the electrocatalyst, $[Ru(Mebimpy)(4,4'\text{-}((HO)_2OPCH_2)_2bpy)(OH_2)]^{2+}$ (Mebimpy = 2,6-bis(1-methylbenzimidazol-2-yl)pyridine; bpy = 2,2′-bipyridine) (**1-PO$_3$H$_2$**) to give RVC|*nano*ITO-Ru^{II}-OH_2^{2+}. The redox properties of the catalyst are retained on the electrode surface. Electrocatalytic oxidation of benzyl alcohol to benzaldehyde occurs with a 75% Faradaic efficiency compared to 57% on *nano*ITO. Electrocatalytic water oxidation at 1.4 V vs SCE on derivatized RVC|*nano*ITO electrode with an internal surface area of 19.5 cm^2 produced 7.3 μmoles of O_2 in 70% Faradaic yield in 50 min.

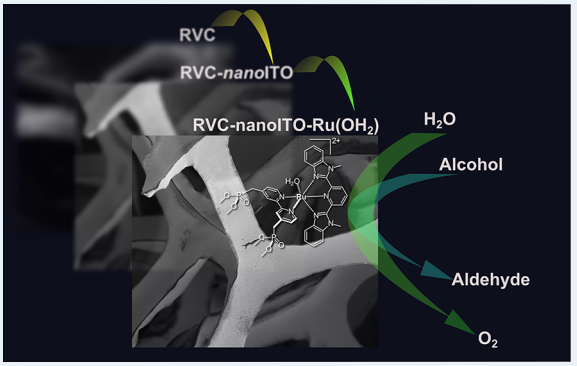

KEYWORDS: *electrocatalysis, reticulated vitreous carbon, nanoITO, high surface area, polypyridyl ruthenium complex, water oxidation*

Nanostructured, transparent conducting oxide (TCO) films, for example, Sn^{IV}-doped In_2O_3 (ITO) or fluoride-doped SnO_2 (FTO), have properties potentially exploitable in a variety of applications from electrochromic displays to artificial photosynthesis. Surface-derivatized *nano*ITO, which is an n-type TCO with a wide potential window,[1] has been applied to electrocatalytic water oxidation,[2] oxidation of metal complexes,[3] and oxidation of organics[4] by surface-bound molecular catalysts, in fundamental studies of interfacial proton-coupled electron transfer (PCET).[5] Surface-derivatization is also of crucial importance for TiO_2 photosensitization in dye-sensitized solar cells (DSSC).[6]

Electrochemical studies on the surface-bound catalyst $[Ru(Mebimpy)(4,4'\text{-}((HO)_2OPCH_2)_2bpy)(OH_2)]^{2+}$ (Mebimpy = 2,6-bis(1-methylbenzimidazol-2-yl)pyridine; bpy = 2,2′-bipyridine) (**1-PO$_3$H$_2$**) on planar ITO and FTO electrodes, Figure 1, have shown that redox potentials, pH dependences, catalytic properties, and water oxidation mechanism are all retained on oxide surfaces. In electrocatalytic applications, current densities are limited by the relatively small number of catalyst sites with closely packed surface loadings of $\Gamma \sim 1.2 \times 10^{-10}$ mol cm^{-2}. Marginally enhanced currents were obtained by loading the catalyst on ~5 μm thick, nanostructured films of TiO_2 (*nano*TiO_2) on ITO. Even given the three-dimensional character of the films, and significant increase in the number of catalyst sites with $\Gamma = 5.3 \times 10^{-8}$ mol cm^{-2}, only a modest current density enhancement of ~3.5, was observed. On the semiconductor surface catalyst, oxidative activation of the catalyst occurs by cross-surface electron transfer since the potential(s) for oxidative activation lie within the band gap.[7]

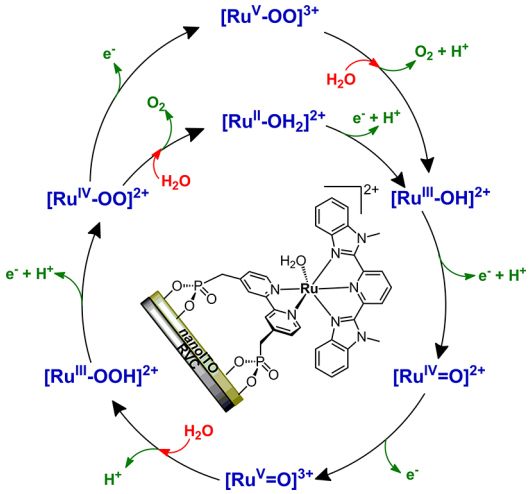

Figure 1. Structure of $[Ru(Mebimpy)(4,4'\text{-}((HO)_2OPCH_2)_2bpy)(OH_2)]^{2+}$ on nanoITO illustrating the stepwise mechanism for water oxidation.

Recently, we reported enhanced current densities for water oxidation by **1-PO$_3$H$_2$** bound to high surface area *nano*ITO

Received: May 14, 2013
Revised: June 27, 2013
Published: July 3, 2013

   dx.doi.org/10.1021/cs4003595 | ACS Catal. 2013, 3, 1850−1854

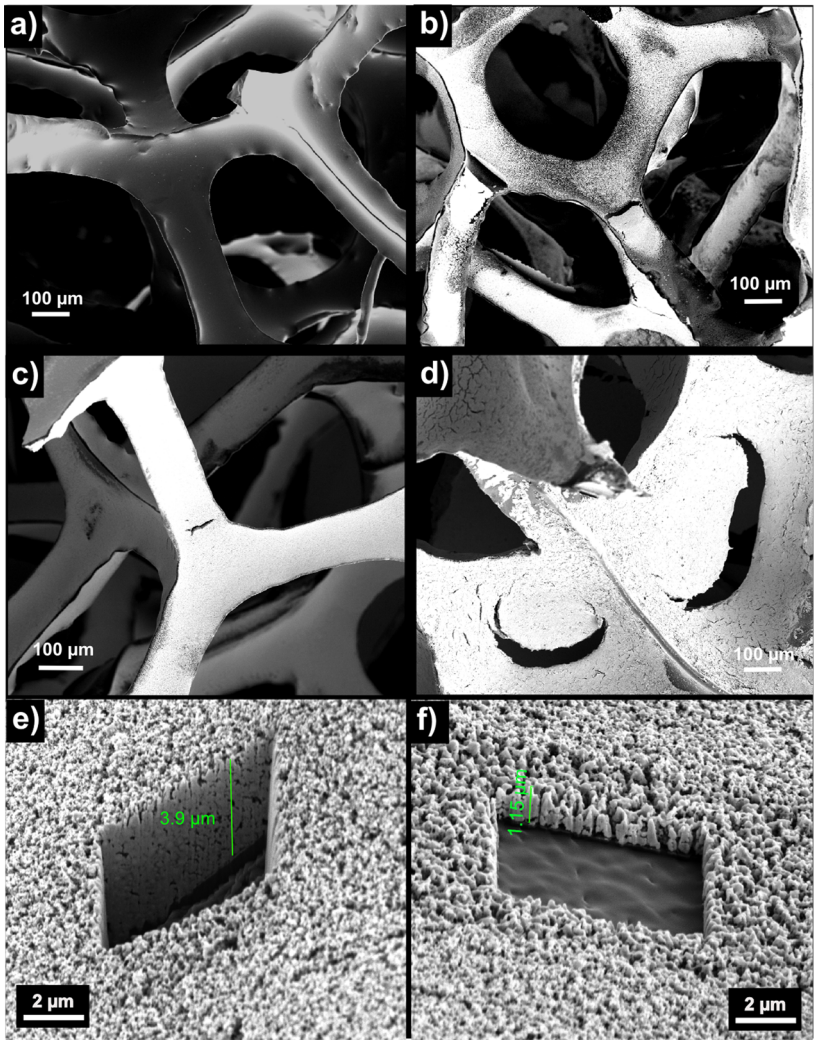

Figure 2. SEM micrographs: (a) RVC electrode; (b–d) RVC|*nano*ITO electrodes prepared from suspensions of *nano*ITO, (b) 10, (c) 100, and (d) 200 mg/mL in ethanol. Cross sections of the electrode in (c) are presented in (e) and (f).

(2.5 μm).[2b] The water oxidation mechanism is shown in Figure 1.[2b,4b] At an applied potential of 1.84 V vs NHE at pH = 5, sustained water oxidation catalysis occurred with a current density of 0.17 mA cm^{-2} and a turnover rate of 0.027 s^{-1} with no decrease in current density after 8 h. Compared to planar ITO, the current density was enhanced by 11-fold.

A key to enhanced current densities in electrocatalytic applications is to increase the surface area-to-volume ratio. An appealing electrode material for this purpose is reticulated vitreous carbon (RVC). RVCs have surface-to-volume ratios that are typically >10 cm^2 cm^{-3}, and are relatively inexpensive.[8] They have been applied in flow electrochemical reactors,[9] lead-acid batteries,[10] electroanalysis,[9a,11] and bioremediation.[10,12]

We report here a novel, hybrid approach to achieving higher surface area-to-volume ratios. It combines high surface area RVC electrodes with a stable overlayer of *nano*ITO followed by surface derivatization. The resulting hybrid electrodes provide a flexible platform for a variety of potential applications in analysis and electrocatalysis.

RVC electrodes (pores/inch = 45; porosity: 96.5%; bulk density: 0.048 g cm^{-3}; 10 × 10 × 6 mm) were purchased from ER&G Aerospace. Geometric surface areas were calculated according to eq 1,[13]

$$A^{\mathrm{RVC}}(\mathrm{cm}^2) = \frac{m^{\mathrm{RVC}}(\mathrm{g})}{d(\mathrm{g/cm}^3)} \times \frac{A}{V}(\mathrm{cm}^2/\mathrm{cm}^3) \quad (1)$$

with m^{RVC} the electrode mass, A/V the surface area to volume ratio (29.7 cm^2/cm^3 for 45 p.p.i. RVC),[8] and d the density. RVC electrodes were modified by overlayers of *nano*ITO by dip-coating in suspensions of different concentrations of ITO nanoparticles (Aldrich, < 50 nm particle size) in ethanol. After a 10 min immersion, the electrodes were removed and annealed in a tube furnace in a N_2 atmosphere 5% in H_2 at 500 °C. Dip-coating methodology was chosen given its simplicity and well-documented applicability to the deposition of ITO thin films either from soluble precursors[14] or directly from ITO nanoparticle suspensions.[15]

Film thicknesses were evaluated by focused ion beam (FIB) patterning with the influence of nanoparticle concentration on film coverage shown in Figure 2.

The dip-coating procedure from 10 mg mL^{-1} suspensions, (b) in Figure 2, gave uneven coverages and discontinuous film formation. Complete coverage was achieved with 100, (c), and 200 mg mL^{-1} (d) suspensions. However, by 200 mg mL^{-1}, ITO particles accumulate and block the pores after annealing. Optimal properties were obtained at 100 mg mL^{-1} with maximized film coverage free of pore blocking.

dx.doi.org/10.1021/cs4003595 | *ACS Catal.* 2013, 3, 1850–1854

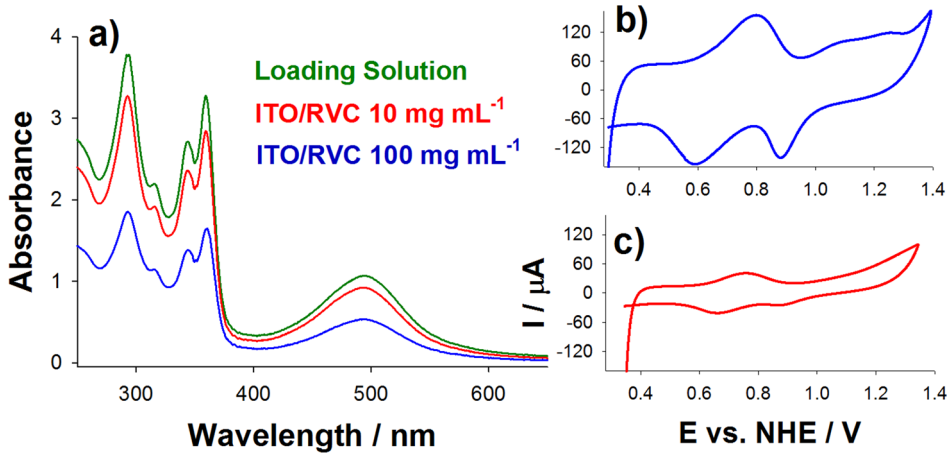

Figure 3. (a) UV−visible absorption spectra of **1-PO_3H_2**, 0.1 mM in methanol (violet), before and after loading RVC|*nano*ITO to give RVC|*nano*ITO-Ru^{II}-OH_2^{2+}. Loadings were from suspensions of 100 (blue) and 10 (red) mg mL^{-1} of *nano*ITO in ethanol. Cyclic voltammograms in an acetate buffer at pH 5 (I = 0.1) at 5 mV s^{-1} are shown in (b) and (c), respectively. RVC area = 19.5 cm^2.

Analysis of film thickness by FIB patterning revealed films with thicknesses from 1 to 4 μm, Figures 2e and f. The thickness variations observed are due to local morphological variations in the RVC substrates. ITO suspensions accumulated in valleys with less liquid retained at the edges. Local structural features and mass gains with oxide addition were reproducible. Loading with suspensions of 100 mg mL^{-1} resulted in mass gains of 64 ± 3%.

Effective surface areas were evaluated by use of cyclic voltammetry (CV) and measurements on the $Fe(CN)_6^{3-/4-}$ couple, Supporting Information, Figure S1. This couple is reversible on glassy carbon and RVC electrodes appearing at 0.45 V vs NHE. Peak currents on RVC|*nano*ITO were enhanced by a factor of ~3 relative to RVC while the peak separation remained constant at 68 mV at 10 mV s^{-1}. Therefore, the current enhancement observed is attributed to an increase in electroactive surface area for the overlayer structure. Simultaneous energy dispersive X-ray spectroscopy (EDS) measurements confirmed the presence of the oxide overlayer with no evidence for carbon inclusion with the stoichiometry of *nano*ITO maintained, Supporting Information.

In a second stage, RVC|*nano*ITO electrodes were functionalized by adding **1-PO_3H_2**. The synthesis of **1-PO_3H_2** was reported elsewhere.[16] Loading of the catalyst on the oxide surface was carried out by immersing the overlayer electrodes in a 0.1 mM solution of **1-PO_3H_2** in methanol for 3 h.

As expected, the extent of catalyst loading to RVC|*nano*ITO increases with the amount of ITO in the overlayer. Figure 3a shows UV−visible spectra of loading solutions before (violet) and after contact with RVC|*nano*ITO. Based on absorbance changes in the loading solutions at 495 nm before and after loading, suspensions of 10 and 100 mg mL^{-1} gave loadings of Γ_{UV-vis} = 1.38 nmol/cm^2 and Γ_{UV-vis} = 5.12 nmol/cm^2, respectively.

A similar trend is observed in the CV measurements in Figure 3b,c on the resulting RVC|*nano*ITO-Ru^{II}-OH_2^{2+} electrodes. A broad, scan dependent wave for the Ru^{III}-OH^{2+}/Ru^{II}-OH_2^{2+} couple appears at $E_{1/2}$ = 0.77 V vs NHE with a peak-to-peak separation of ΔE_p = 200 mV at 5 mV/s, Supporting Information. Wave shapes and ΔE_p values are distorted compared to an ideal surface couple because of high catalyst loadings, local heterogeneities, and slow intrafilm electron transfer.

Within the same potential window, a further broad oxidative wave is observed at $E_{p,a}$ = 1.1 V for the Ru^{IV}=O^{2+}/Ru^{III}-OH^{2+} couple. As observed earlier on *nano*ITO, this couple is kinetically inhibited by the kinetic requirement for proton loss from Ru^{III}-OH^{2+}.[3b] At 1.24 V, a second, broad oxidation wave is observed of comparable peak current. It arises from direct oxidation of Ru^{III}-OH^{2+} to $Ru^{IV}(OH)^{3+}$, eq 2, followed by deprotonation, eq 3. The narrow, re-reduction wave at $E_{p,c}$ = 0.88 V arises from Ru^{IV}=O^{2+} re-reduction to Ru^{III}−O^{2+} followed by rapid protonation to give Ru^{III}-OH^{2+}.

$$Ru^{III}\text{-}OH^{2+} \xrightarrow{-e^-} Ru^{IV}(OH)^{3+} \quad (2)$$

$$Ru^{IV}(OH)^{3+} \xrightarrow{-H^+} Ru^{IV}{=}O^{2+} + H^+ \quad (3)$$

The extent of surface loading of electrochemically active **1-PO_3H_2** was determined by integration of the Ru^{II}-OH_2^{2+}→ $Ru^{III}OH^{2+}$ oxidation wave at 5 mV/s. Integration gave $\Gamma_{e\text{-}chem}$ = 0.22 nmol/cm^2 from a suspension of 10 mg mL^{-1} and $\Gamma_{e\text{-}chem}$ = 1.2 nmol/cm^2 from 100 mg mL^{-1}. Comparison of loadings from UV−visible and electrochemical measurements showed that 16% of the sites on RVC|*nano*ITO-Ru^{II}-OH_2^{2+} from the 10 mg mL^{-1} suspension were electroactive and 23% from the 100 mg/mL^{-1} suspension. This result shows that only a small fraction of catalyst sites are electrochemically accessible even at the slow scan rate of 5 mV/s. CV measurements at slow scan rates were preferred to differentiate the multiple processes appearing in the voltammetric wave forms. However, functionalized nanoITO/RVC electrodes exhibit the expected linear behavior of the peak current as function of scan rate in the range between 2 to 20 mV/s (Supporting Information, Figure S4).

In an earlier study, electrocatalytic oxidation of benzyl alcohol to benzaldehyde by *nano*ITO-Ru^{II}-OH_2^{2+} was investigated. In that study it was found that oxidation by *nano*ITO-Ru^{IV}=O^{2+} was slow with $k_{Ru^{IV}=O^{2+}}$ = 1.3 ± 0.02 × 10^{-2} M^{-1} s^{-1} while oxidation by *nano*ITO-$Ru^{IV}(OH)^{3+}$ occurs with $k_{Ru^{IV}(OH)^{3+}}$ = 11.1 ± 0.4 M^{-1} s^{-1} with a C-H/C-D kinetic isotope effect (KIE) of 3.[4b] Because of this large difference in catalytic rate constants for *nano*ITO-Ru^{IV}=O^{2+} and *nano*ITO-$Ru^{IV}(OH)^{3+}$, significant current enhancements on nanoITO on FTO glass electrodes were only observed where *nano*ITO-$Ru^{IV}(OH)^{3+}$ was produced.

dx.doi.org/10.1021/cs4003595 | *ACS Catal.* 2013, 3, 1850−1854

Figure 4 shows the voltammetric response of RVC|*nano*ITO-Ru^{II}-OH_2^{2+} in an acetate buffer at pH 5 (I = 0.1) with and

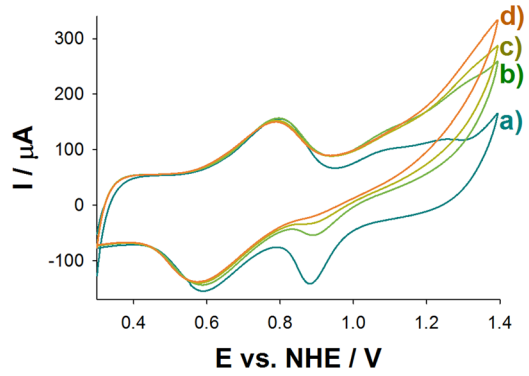

Figure 4. Cyclic voltammograms at a RVC|*nano*ITO-Ru^{II}-OH_2^{2+} electrode in acetate buffer pH 5 (I = 0.1) at 5 mV/s with (a) 0, (b) 1.5, (c) 3.0, and (d) 5.9 mM of added benzyl alcohol. RVC area = 19.5 cm^2.

without added benzyl alcohol. It is notable that, in contrast to *nano*ITO-Ru^{II}-OH_2^{2+}, significant catalytic enhancement occurs at potentials as low as 0.89 V with RVC|*nano*ITO-Ru^{IV}=O^{2+} as oxidant. This is an impressive manifestation of the increased concentration density of catalyst sites; no enhancement is observed for *nano*ITO-Ru^{IV}=O^{2+} under the same conditions.[4b] At 5 mV/s, oxidation by RVC|*nano*ITO-Ru^{IV}=O^{2+} is incomplete with additional current enhancement at ~1.24 V because of oxidation of the alcohol by RVC|*nano*ITO-$Ru^{IV}(OH)^{3+}$. Oxidative scans to the RVC|*nano*ITO-$Ru^{IV}(O)^{2+}$→ RVC|*nano*ITO-$Ru^{V}(O)^{3+}$ wave at $E_{p,a}$ ≈ 1.4 V initiates water oxidation by the cycle in Figure 1.

$$\text{RVC|}nano\text{ITO-Ru}^{IV}\text{=O}^{2+} + \text{PhCH}_2\text{OH} \rightarrow \text{RVC|}nano\text{ITO-Ru}^{II}(\text{OH}_2)^{2+} + \text{PhCHO} \quad (2)$$

Oxidation of 20 mM benzyl alcohol in acetate buffer at pH 5 (I = 0.1) by controlled potential electrolysis at 1.24 V vs. NHE at *nano*ITO-Ru^{II}-OH_2^{2+} (1 cm^2) for 16 h occurred with passage of 1.5 C giving 4.4 μmoles of benzaldehyde in 57% Faradaic yield.[4b] As shown in the current−time curves in Supporting Information. Given the much larger area of the RVC|*nano*ITO-Ru^{II}-OH_2^{2+} electrodes and increased number of catalytic sites compared to *nano*ITO-Ru^{II}-OH_2^{2+}, a 30 mM solution of benzyl alcohol, instead of 20 mM, was electrolyzed at 1.24 V vs. NHE to avoid significant depletion in the total concentration of the substrate during the course of the electrolysis. After a time lapse of 2.2 hours, 1.2 C were passed producing 4.7 μmoles of benzaldehyde with a Faradaic efficiency of 75% (TON = 402, TOF = 0.05 s^{-1}). The results of the two experiments are comparable even given the difference in benzyl alcohol concentration. Catalytic currents increase linearly up to 10 mM but then reach a plateau.

Water oxidation catalysis is also greatly enhanced on RVC|*nano*ITO-Ru^{II}-OH_2^{2+} thanks to the increased total number of catalytic sites. Controlled potential electrolysis in 0.1 M $HClO_4$ at 1.64 V vs. NHE, past $E_{p,a}$ for oxidation of -Ru^{IV}=O^{2+} to -$Ru^{V}(O)^{3+}$, occurred with the passage of 4 C after 50 min of electrolysis, Supporting Information. GC-FID measurements on a headspace sample showed formation of ~7.3 μmoles of O_2 and a Faradaic yield of 70%, which is equivalent to a TON = 1248 and TOF = 0.42 s^{-1}. The electrolysis current was stable at 1.4 mA (73 μA/cm^2) over the course of the electrolysis demonstrating the stability of the electrode toward sustained water oxidation. In both cases, Faradaic efficiencies below 100% can be attributed to either catalyst decomposition followed by desorption or oxidation of exposed carbon areas.

Since oxidation/degradation of the electrode was not observed under the electrocatalytic conditions describe above, thermal annealing at 500 °C was attempted to accelerate the chemical oxidation of the carbon substrate. These experiments showed that the oxide overlayer stabilizes the RVC toward oxidation. A RVC electrode heated in air at 500 °C for 1 h resulted in 49% loss of the initial mass with noticeable loss of mechanical strength. Under the same conditions, an RVC|*nano*ITO electrode lost only 16% of its initial mass with its mechanical properties largely intact.

In summary, our results demonstrate successful implementation of an important strategy for obtaining enhanced current densities by an overlayer strategy based on TCO coatings on RVC. Although potentials and properties of individual sites in the resulting derivatized structures of RVC|*nano*ITO-Ru^{II}-OH_2^{2+} are relatively unchanged, and a large fraction of sites are electrochemically inactive, significant current enhancements are obtained for electrocatalytic oxidation of both benzyl alcohol and water. The origin of the current enhancement is in an *increased density of sites in the highly porous structure of the RVC*. The resulting structures offer greatly enhanced currents, shortened electrolysis times, and oxidative stability by use of an approach that may be applicable to a wide variety of conducting and nonconducting framework materials. In particular, we are currently investigating the extension of this strategy to other TCO materials such as FTO, antimony-doped tin oxide (ATO), aluminum-doped zirconium oxide (AZO), and others.

■ ASSOCIATED CONTENT

Supporting Information

ITO coating, catalyst loading procedure, and product analysis of controlled potential electrolysis are given as are current−time profiles. ^{1}H NMR spectra and GC-FID analysis and additional SEM images are also presented. This material is available free of charge via the Internet at http://pubs.acs.org.

■ AUTHOR INFORMATION

Corresponding Author

*E-mail: tjmeyer@email.unc.edu. Fax: +1 919-962- 2388. Phone: +1 919-843-8313.

Notes

The authors declare no competing financial interest.

■ ACKNOWLEDGMENTS

This work was supported by the Center for Catalytic Hydrocarbon Functionalization, an Energy Frontier Research Center (EFRC) funded by the U.S. Department of Energy (DOE), Office of Science, Office of Basic Energy Sciences (BES), under Award DE-SC0001298, supporting M.A.M. Funding from the UNC EFRC: Center for Solar Fuels, an Energy Frontier Research Center, funded by U.S. DOE-BES, under Award DE-SC0001011, supporting J.J.C. is gratefully acknowledged. L.A. wishes to acknowledge financial support from the Research Triangle Solar Fuels Institute (RTSFI).

REFERENCES

(1) Bel Hadj Tahar, R.; Ban, T.; Ohya, Y.; Takahashi, Y. *J. Appl. Phys.* **1998**, *83*, 2631.

(2) (a) Concepcion, J. J.; Jurss, J. W.; Hoertz, P. G.; Meyer, T. J. *Angew. Chem., Int. Ed.* **2009**, *48*, 9473. (b) Chen, Z.; Concepcion, J. J.; Hull, J. F.; Hoertz, P. G.; Meyer, T. J. *Dalton Trans.* **2010**, *39*, 6950. (c) Chen, Z.; Concepcion, J. J.; Luo, H.; Hull, J. F.; Paul, A.; Meyer, T. J. *J. Am. Chem. Soc.* **2010**, *123*, 17670. (d) Hoertz, P. G.; Chen, Z.; Kent, C. A.; Meyer, T. J. *Inorg. Chem.* **2010**, *49*, 8179.

(3) Elliott, C. M.; Caramori, S.; Bignozzi, C. A. *Langmuir* **2005**, *21*, 3022.

(4) (a) Paul, A.; Hull, J. F.; Norris, M. R.; Chen, Z.; Ess, D. H.; Concepcion, J. J.; Meyer, T. J. *Inorg. Chem.* **2011**, *50*, 1167. (b) Vannucci, A. K.; Hull, J. F.; Chen, Z.; Binstead, R. a.; Concepcion, J. J.; Meyer, T. J. *J. Am. Chem. Soc.* **2012**, *134*, 3972. (c) Vannucci, A. K.; Chen, Z.; Concepcion, J. J.; Meyer, T. J. *ACS Catal.* **2012**, *2*, 716.

(5) (a) Gagliardi, C. J.; Jurss, J. W.; Thorp, H. H.; Meyer, T. J. *Inorg. Chem.* **2011**, *50*, 2076. (b) Gagliardi, C. J.; Westlake, B. C.; Kent, C. A.; Paul, J. J.; Papanikolas, J. M.; Meyer, T. J. *Coord. Chem. Rev.* **2010**, *254*, 2459.

(6) Brown, D. G.; Schauer, P. a.; Borau-Garcia, J.; Fancy, B. R.; Berlinguette, C. P. *J. Am. Chem. Soc.* **2013**, *135*, 1892.

(7) Chen, Z.; Concepcion, J. J.; Jurss, J. W.; Meyer, T. J. *J. Am. Chem. Soc.* **2009**, *131*, 15580.

(8) Friedrich, J. M.; Ponce-de-León, C.; Reade, G. W.; Walsh, F. C. *J. Electroanal. Chem.* **2004**, *561*, 203.

(9) (a) Curran, D. J.; Tougas, T. P. *Anal. Chem.* **1984**, *56*, 672. (b) Zhu, C.; Curran, D. J. *Electroanalysis* **1991**, *3*, 511.

(10) Recio, F. J.; Herrasti, P.; Sirés, I.; Kulak, A. N.; Bavykin, D. V.; Ponce-de-León, C.; Walsh, F. C. *Electrochim. Acta* **2011**, *56*, 5158.

(11) Sorrels, J. W.; Dewald, H. D. *Anal. Chem.* **1990**, *62*, 1640.

(12) Arredondo Valdez, H. C.; García Jiménez, G.; Gutiérrez Granados, S.; Ponce de León, C. *Chemosphere* **2012**, *89*, 1195.

(13) Frydrychewicz, A.; Yu, S.; Tsirlina, G. A.; Jackowska, K. *Electrochim. Acta* **2005**, *50*, 1885.

(14) (a) Seki, S.; Sawada, Y.; Nishide, T. *Thin Solid Films* **2001**, *388*, 22. (b) Nishio, K.; Sei, T.; Tsuchiya, T. *J. Mater. Sci.* **1996**, *31*, 1761. (c) Graberg, T. V.; Hartmann, P.; Rein, A.; Gross, S.; Seelandt, B.; Röger, C.; Zieba, R.; Traut, A.; Wark, M.; Janek, J.; Smarsly, B. M. *Sci. Technol. Adv. Mater.* **2011**, *12*, 025005.

(15) Mahajeri, M.; Voigt, M.; Klupp Taylor, R. N.; Reindl, a.; Peukert, W. *Thin Solid Films* **2010**, *518*, 3373.

(16) Concepcion, J. J.; Jurss, J. W.; Norris, M. R.; Chen, Z.; Templeton, J. L.; Meyer, T. J. *Inorg. Chem.* **2010**, *49*, 1277.